

Combustion thermoacoustics: on the relevance of some stability criteria

Jean-Michel Klein^{*†}, Aurelien Genot^{*}, Axel Vincent-Randonnier^{*}, Arnaud Mura^{**}

^{*}DMPE, ONERA, Université Paris Saclay, F-91123 Palaiseau - France

^{**}Institut Pprime, 2 Bd des Frères Lumière, Chasseneuil-du-Poitou 86360, France

jean-michel.klein@onera.fr

[†]Corresponding author

Abstract

Combustion instabilities in a backward-facing step combustor are numerically studied to assess the relevance of some criteria for thermoacoustic instability: the classical Rayleigh criterion, the extended Chu criterion, and generalized non-linear criteria. Two cases are simulated: (i) a stable case where the flame is successfully anchored at the step with oscillations induced by the coupling with the intrinsic shear-layer instability (ii) an unstable case, where the excitation of longitudinal acoustic modes is triggered, and a flame-hydrodynamic-acoustic coupling leads to an instability featuring periodic flame flashback, resulting in large amplitude flame motion, pressure, velocity, and temperature oscillations. For the stable case, linearization is possible due to small levels of fluctuations and the non-linear criteria can simply be decomposed into the Chu criterion, and an additional damp term. The Rayleigh criterion fails to describe destabilization which occurs on the stable case, featuring only an intrinsic hydrodynamic instability and no acoustic feedback. The non-linear criterion describes properly the mechanisms which have a major role in both case: stabilization through burnt gas recirculation, destabilization with the flame being convected in fresh reactants regions. The flashback being driven by acoustic waves crossing the reaction zone, the computed values of the Rayleigh criterion, which describes those couplings displays large variation peaks at those instants. The extended non-linear criterion is however necessary to describe properly the mechanisms related to the flashback: its initiation results from the conversion of acoustic energy into fluctuating energy, its development from the production of fluctuating energy, and its blow-off from this fluctuating energy being reconverted into acoustic energy.

1. Introduction

When designing modern propulsion systems, major concern is the flame destabilization in the combustion chamber [21], especially in ramjet combustors [18, 10] where incoming flow velocity (several tens of meters per second), is far greater than propagation speed of the premixed flame front (generally below one meter per second [43]). A common way to stabilize combustion in these engines consists in flame holder implementation [16]. The flame is thus anchored on the generated wake through burnt gas recirculation. Unfortunately, introducing an aerodynamic obstacle promotes several hydrodynamic instabilities due to the flow shearing [8]. Moreover, the combustor boundaries generally reflecting acoustic waves, thus exciting acoustic modes, can also trigger thermoacoustic instabilities [35] (feedback between unsteady heat release and pressure oscillations). The coupling of unsteady flames with hydrodynamic instabilities can trigger large amplitude pressure oscillations and flame motion [23]. This phenomena can damage the combustor, induce flashback [15, 17], and may even extinct the flame [39].

Studies about thermoacoustic instabilities often focus on the phase shift between pressure (p_1) and heat release ($\dot{\omega}_{T1}$) oscillations, as it enables studying the Rayleigh criterion [34]. According to this criterion, a combustor is unstable if its linear acoustic energy [37] $E_{ac} = p_1^2 / (2\gamma_0 p_0) + (\rho_0 / 2) \mathbf{v}_1^2$ is growing, which can be reformulated:

$$\mathcal{D}_{Rayl} = \iiint_{\Omega} \frac{\gamma_0 - 1}{\gamma_0 p_0} p_1 \dot{\omega}_{T1} > \mathcal{L} \quad (1)$$

with \mathcal{D}_{Rayl} being the Rayleigh index. For the unstable conditions, its integral over the combustor volume Ω has to be greater than the acoustic losses \mathcal{L} . The ${}_1$ subscript applies to variables fluctuations around its reference

(time averaged) value $\bar{\rho}_0$, \mathbf{v}_1 is thus the velocity oscillation whereas γ_0 and ρ_0 stand for the Laplace coefficient and density of the reference values.

However, considering only acoustic energy in some flows including entropy fluctuations can lead to contradictions where the acoustic energy grows whereas the flow stabilizes [28, 11]. Unsteady combustion being non-isentropic due to the large temperature gap between fresh and burnt gases [40], a fluctuating energy $E_f = p_1^2/(2\gamma_0\rho_0) + (\rho_0/2)\mathbf{v}_1^2 + (\rho_0 T_0/c_{p0})s_1^2$, which includes entropy fluctuations s_1 (c_p is the constant pressure heat capacity) seems more relevant to describe flame oscillations. This energy formalism modifies Eq. (1), leading to the Chu criterion [6]:

$$\mathcal{D}_{Chu} = \iiint_{\Omega} \frac{1}{T_0} T_1 \omega_{T1} > \mathcal{L} \quad (2)$$

by introducing Chu's index \mathcal{D}_{Chu} , which states that one should study the coupling between the heat release ($\dot{\omega}_{T1}$) and temperature (T_1).

Temperature and entropy oscillations are only limited by the gas expansion ratio $\tau = (\rho_u - \rho_b)/\rho_b$ (subscripts b and u denote burnt and unburnt gases). As it is generally far greater than unity, these oscillations are highly prone to non-linearities [12]. Linear perturbation energies defined above may thereby not be sufficient to quantify instabilities in cases where large scale flame motion is present and burnt gases are pushed in flow regions whose mean temperature T_0 is significantly smaller than the burnt gas temperature T_b .

In 1996, Myers [26] proposed a method to derive a non-linear disturbance energy for gaseous mono-species flow, whose linearization yields to known acoustic and fluctuating energies [24]. In 2006, Giauque *et al.* [12] extended this framework to multi-component reacting flow, highlighting a non linear thermo-acoustic criterion, among plenty other terms describing other types of feedback.

Due to the difficulty for experiments to fully quantify the quantities related to these extended criteria, high-fidelity numerical simulation of compressible reactive flows [36], where each variable can be accessed at any time and location, thus appears as a promising way to compute and study them.

The current paper focuses on thermoacoustic coupling effect in a backward-facing-step combustor [3]. Figure 1 depicts the flame anchoring mechanisms in such a combustor. As a parallel flow containing the reactants crosses a combustion chamber with a sudden expansion, boundary layer detachment takes place at the edge of the step, leading to a recirculating bubble with subsequent re-attachment [5]. The flame can thus anchor to the shear-layer and stable combustion is possible [21]. The only source of instability is the intrinsic shear-layer instability [8]. However, when the combustor boundaries reflect acoustic waves, unstable regimes may be triggered, some of them

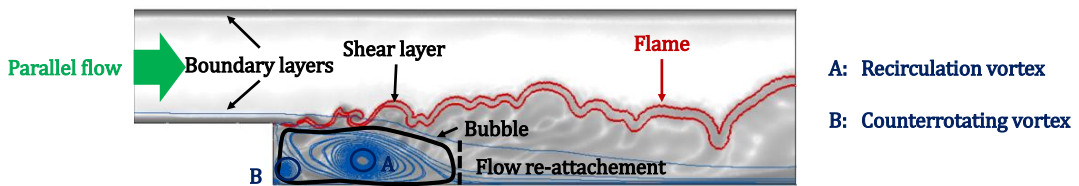


Figure 1: Flow structure on a backward-facing step flame-holder.

featuring periodic flame flashback [17, 1], which is indeed a massive flame motion, prone to non-linearities.

The paper is organised as follows. Section 2 presents numerical simulations of combustion in a backward-facing step configuration. Both a stable and an unstable (with flashback) regimes are computed. Several criteria for thermoacoustic instabilities are then computed and studied for both cases in section 3.

2. Numerical simulations

The present study was performed using ONERA's in house computational fluid dynamics code CEDRE [36, 22, 25], using a finite volume solver for compressible multi-component reactive flows.

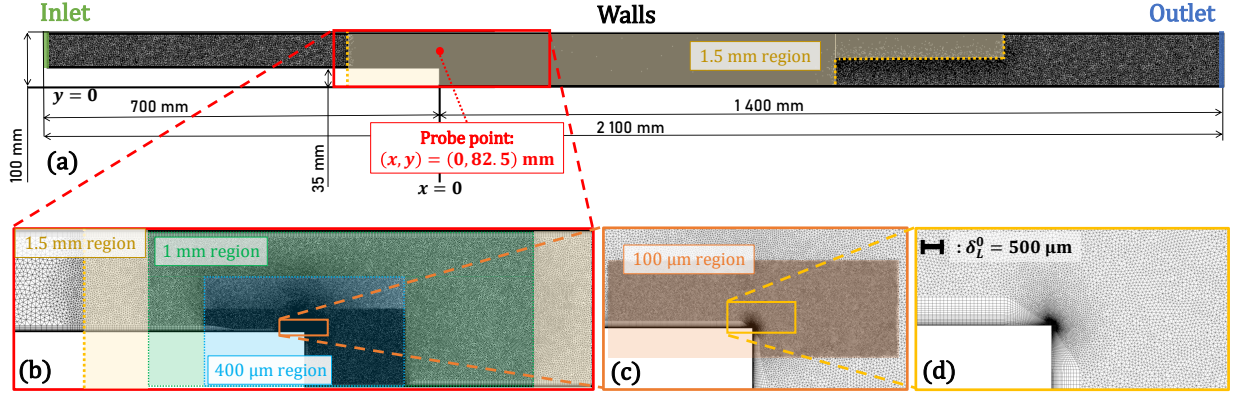


Figure 2: Computational mesh description. (a): Geometry with dimensions and mesh overview, (b): Refinement around the step, $\Delta x < 1$ mm for $x \in [-100; 150]$ mm, $\Delta x < 400$ μ m for $(x, y) \in [-45; 65] \times [0; 50]$ mm. (c): $\Delta x < 100$ μ m for $(x, y) \in [-15; 15] \times [3.2; 40]$ mm. (d): Boundary layer mesh and size comparison to the laminar flame thickness.

2.1 Computational domain and meshing

The numerical simulations were achieved for operating conditions corresponding to the MICAEDI/LAERTE setup [3, 38, 29], considering a region where the inlet flow is homogeneous and inlet gases are perfectly premixed (*i.e.* negligible equivalence ratio fluctuations). Inlet and outlet nozzles are not modelled and simplified acoustic boundary conditions are applied. An overview of the computational domain and its dimensions are given in Figure 2.a). The unstructured 2D-mesh contains 352 686 cells and is composed of triangles with quad layers at the walls vicinity. Figures 2.b–d) display enlarged views of the mesh which has been refined around the backward-facing step, with cells sizes of 1 mm, 400 μ m, and 100 μ m (Fig. 2.b-c). The prismatic cells above the wall can be seen on Fig. 2.d), their minimal size is $\Delta y = 5$ μ m.

In order to quantify the viscous and thermal boundary layer meshing quality, the first mesh cell size can be made non-dimensional through the quantities Δy^+ and Δy^{++} [33], whose expressions are:

$$\Delta y^+ = \frac{\Delta y u_\tau}{\nu} \quad \text{and} \quad \Delta y^{++} = \frac{\Delta y u_\tau}{a} \quad \text{with} \quad u_\tau = \sqrt{\frac{\tau_w}{\rho}} \quad (3)$$

With τ_w the wall viscous stress, ν the dynamical viscosity, and a the thermal diffusivity, these two dimensionless quantities are inter-related through the Prandtl number such as: $\Delta y^{++} = Pr \Delta y^+$. *A posteriori* analysis of the numerical simulations shows that the maximal values are $\max(\Delta y^+) = 0.5$ and $\max(\Delta y^{++}) = 0.36$, *i.e.* smaller than unity, which is convenient to properly resolve the wall-bounded turbulent flow [31].

2.2 Numerical modelling

The present numerical simulations are conducted within the large-eddy simulation (LES) framework [30], where filtered Navier-Stokes equations are used and the largest scales of the flow are explicitly computed whereas the subgrid-scales (SGS), which are too small to be resolved with the mesh cells sizes, are modelled. The wall-adapting local eddy (WALE) [27] model is used to represent the unresolved scales of turbulence.

The inlet boundary corresponds to a methane-air mixture at equivalence ratio $\phi = 0.8$, whose temperature is $T_{in} = 520$ K. The imposed axial velocity $V_0 = 50$ m/s results in reflecting acoustic waves. Atmospheric pressure $p_{x=L} = 100400$ Pa is set at the outlet. The wall temperature is set to $T_w = 300$ K.

Chemical reaction is described with a single-step chemistry model, involving methane (CH_4), oxygen (O_2), carbon dioxide (CO_2) and water vapor (H_2O), (nitrogen (N_2) being inert), the relevance of which for studying premixed flame dynamics has been assessed elsewhere (e.g., [9]):



Molecular transport is modelled by assuming constant Schmidt numbers together with a constant mixture Prandtl number the value of which has been set from a preliminary one-dimensional flame computation performed with the same single-step chemistry model but using the CANTERA solver [14]. Table 1 summarizes the retained values.

Schmidt Numbers Sc_k					Prandtl
CH_4	O_2	N_2	CO_2	H_2O	number Pr
0.69	0.79	0.73	0.95	0.55	0.71

Table 1: Gas diffusive properties

A Sutherland relation and temperature-based polynomials are used to represent the changes of the species viscosities and thermal capacities. In addition to this, in order to improve the flame-flow coupling in the regions far from the step, where the mesh elements size exceeds the reaction zone length, the flame front is artificially thickened using the TFLES model, with the first efficiency function of Volpiani *et al.* [42], and the sensor of Legier *et al.* [20]. The model has been calibrated to get at least 5 mesh points in the flame front. The temporal integration is performed with a second-order implicit Runge-Kutta scheme [4] with a 5×10^{-8} s time step. Finally, spatial discretization makes use of a second-order multislope MUSCL scheme [19].

A probe point, where the flow properties are extracted every 10^{-6} s has been placed at $(x, y) = (0, 82.5)$ mm, which corresponds to the center of the inlet channel, at the step location (fig. 2.a)).

2.3 Results

The figure 3 shows the root mean square (RMS) values of the unsteady temperature T_1 normalized through its time-averaged value T_0 . RMS values, which are used to quantify oscillation levels of any quantity X are defined as:

$$X_1^{RMS} = \sqrt{\frac{1}{t_f - t_i} \int_{t_i}^{t_f} (X(t) - X_0)^2 dt} \quad (5)$$

$t_f - t_i$ being the time interval over which the averaging is done. In order to post-process the simulation data later in this study, instantaneous 2D fields were exported over a time interval of 40 ms. A resolution of 10^{-5} s has been used, corresponding to 4000 instantaneous 2D fields. Mean temperature isolines $T_0 \in \{650, 1200, 1500, 1900\}$ K are also plotted in Fig. 3 in order to estimate the flame flapping zone.

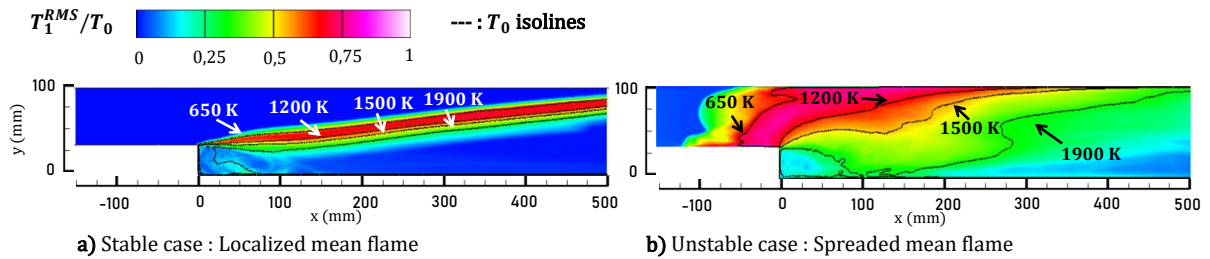


Figure 3: Normalized RMS temperature fluctuations and mean temperature isolines

As emphasized above, two combustion regimes were computed:

- A stable combustion regime, where the outlet reflection coefficient is set to zero thanks to non-reflecting boundary conditions [44]. In this regime, the flame stabilizes and its only motion is due to the shear layer instability (flame wrinkled by vortices). Figure 3.a) shows the spatial distribution of the RMS temperature oscillations normalized by the mean temperature T_0 . In some regions, the temperature oscillation level admits values of T_1^{RMS}/T_1 up to 0.7, which, as addressed in section 1, can compromise the linearization. The mean temperature isolines however admit regular shapes and are constricted, due to the fact that the flame is stabilized and the localized flame limits the spreading of regions with high temperature oscillations. In this simulation, due to the lack of acoustic resonance, the pressure and velocity oscillations remain very small.
- After changing the outlet boundary condition and setting its reflection coefficient value to 1 (*i.e.* the outlet pressure is simply imposed to the atmospheric pressure), combustion becomes unstable. The same quantities as for the stable case are displayed on figure 3.b) for this unstable case. It is obvious that due to a massive flame motion (flashback), which will next be described on figure 5, the flapping zone of the flame is far more spreaded than on the stable case, with high values of T_1^{RMS} (critical for linearization).

As it can be seen on figure 4, which plots the RMS pressure and axial velocity oscillations, respectively normalized through the mean pressure p_0 and the mean speed of sound c_0 , the instability is indeed correlated with pressure and velocity oscillation levels increasing drastically. Both pressure and axial velocity oscillations are principally longitudinal and have maximal amplitudes at the combustor inlet section ($x < 0$ mm). Only the velocity contains some transverse components at the vicinity of the step and at the boundary layers due to dilatation and hydrodynamic effects. The $v_{x1}^{RMS} = v_{x0}$ isoline has also been reported on fig. 4.b), stating that there is a region where the axial velocity is periodically inverted, which develops in the boundary layer and core-flow regions on the unstable case, being indeed prone to flashback.

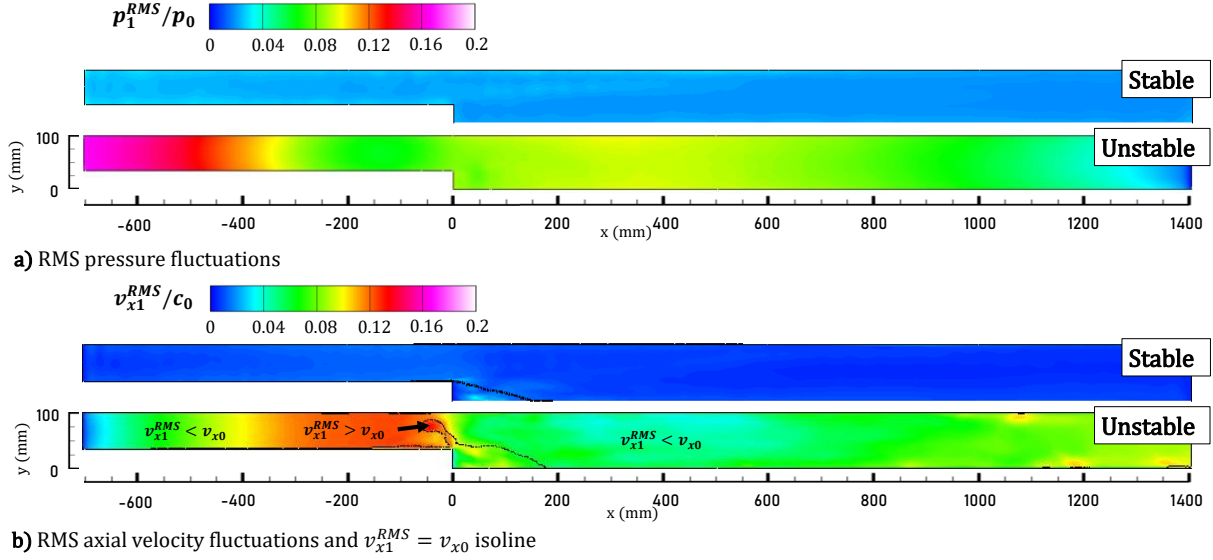


Figure 4: Normalized pressure and velocity RMS fluctuations for both stable and unstable cases

Table 2 compares global properties for both cases. The flame flapping distance Δx_F has been computed by measur-

Regime	Flame flapping	Temperature oscillations T_1^{RMS}/T_0		Pressure oscillations p_1^{RMS}/p_0	
	$\Delta x_F/\delta_L^0$	Mean value	Maximal value	Mean value	Maximal value
Stable	49.3	0.07	0.71	0.02	0.03
Unstable	1341.6	0.17	0.83	0.08	0.17

Table 2: Flame and flow oscillations comparison in stable and unstable cases

ing the maximal distance between the $T_0 = 650$ K and $T_0 = 1900$ K isolines and then non-dimensionalized thanks to the corresponding laminar flame thickness δ_L^0 . For both cases, the RMS temperature maximal levels remain close from each other as they are defined by the fresh-burnt gas temperature gradient (*i.e.* the chemical reaction), but its mean value increases considerably as a direct consequence of the enhanced flame flapping.

Figure 5 finally shows more clearly the flashback cycle mentioned above with 8 snapshots along its 10 ms period, showing the instantaneous Schlieren $||\nabla p||/p$ time evolution, with heat-release rate iso-lines (in red), characterizing respectively the acoustic waves and reaction zones. Major vortices are also reported.

The instantaneous combustion-induced heat release is computed from the species reaction rates $\dot{\omega}_k$ and their standard formation enthalpy $\Delta h_{f,k}^o$ with the following relation:

$$\dot{\omega}_T = - \sum_{k=1}^N \dot{\omega}_k \Delta h_{f,k}^o \quad (6)$$

The isovalue $\dot{\omega}_T = 10^8$ W·m⁻³ is plotted.

The mechanisms leading to flashback once a stable flame is destabilized being described by Keller *et al.* in 1982 [17], the numerical simulation allows a more precise description of the interactions with acoustic waves during limit cycle oscillations. The dynamic can be decomposed into three distinct phases (see fig. 5):

CRITERIA FOR THERMOACOUSTIC INSTABILITY IN COMBUSTORS FEATURING LARGE-SCALE FLAME MOTION

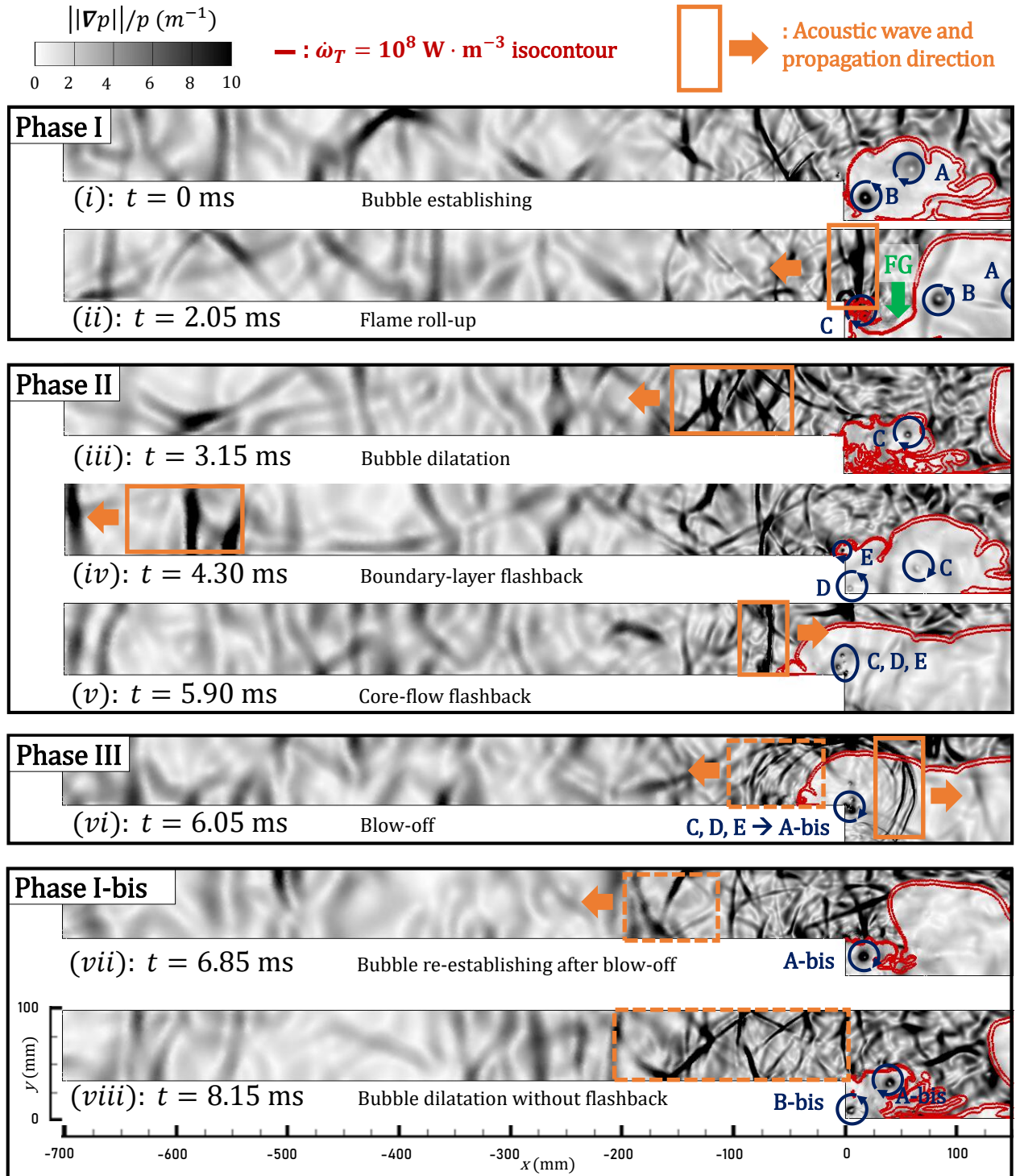


Figure 5: Visualization of the flashback cycle at different phases (6 ms period) : Instantaneous Schlieren ($||\nabla p||/p$ snapshots with heat release (red) and Q criterion (green) isocontours.

- **Phase I** originates from the previous cycle. Recirculation and counterrotating vortices (A) and (B) establish behind the step (i), but do not attach and continue convecting downstream. The convected vortice (B) then stretches the flame, which is then dragged by a newly forming recirculation vortex (C) (ii). Fresh gas (FG) pockets are transported below the step due to this flame rolling-up.
- During **Phase II**, these pockets consumption then provokes the dilatation of the reforming bubble, and thereby the vertical motion of the reaction zone and vortex C (iii). This dilatation couples with a travelling

longitudinal acoustic wave (*ii,iii,iv*), thereby forcing the shedded vortex E (which originates from the boundary layer detachment) upstreams, causing local flow inversion and initiating **boundary layer flashback** [15] (*iv*). The pressure wave being followed with global flow inversion (≈ 3 ms time lag), **core flow flashback** then follows its initiation (*v*).

- During the whole flashback process, the longitudinal wave continues propagating and its direction inverts when it is reflected at the combustor inlet. **Phase III** begins when this wave reaches again the flame (*v*). Being indeed followed by the flow re-inversion, the flashback is very abruptly blown off during this phase (*vi*), and vortices C,D, and E recombine into a new vortex A-bis, leading to a flow topology similar to phase I (*vii*). It can also be seen that the wave divides into transmitted and reflected parts propagating in opposite directions.
- During **Phase I-bis**, the same mechanisms as described in phase I take place, with the difference that no flow inversion occurs during the dilatation of the bubble, whose ascended part is then convected downstream, giving rise to a new phase I.

From this analysis two characteristic frequencies can be identified: (*i*): the bubble dilatation, which occurs two times over a flashback cycle (which has a period of 10 ms), whose characteristic frequency is therefore about 200 Hz (*ii*): the flashback (which occurs every second bubble dilatation, as the coreflow is reversed), has a frequency of approximately 100 Hz. In the next section, a frequency analysis is performed in order to identify more clearly those mechanisms.

2.4 Frequency analysis

Figure 6.a) first shows the recorded dimensionless pressure, velocity and temperature signals at the probe point (see figure 2), for the sake of readability, smoothed signals have been superimposed over the raw pressure and velocity signals. A 40 ms interval (10^{-6} s resolution), corresponding to four flashback signals has been extracted. The flashback is characterized by burnt gases being transported below the step, which is characterized by the temperature signal suddenly increasing. It can be seen that the flashback is indeed correlated with the axial velocity reversal (v_{x1}/c_0 being below the $-v_{x0}/c_0$ line), which appears every second pressure-velocity oscillation cycle. The corre-

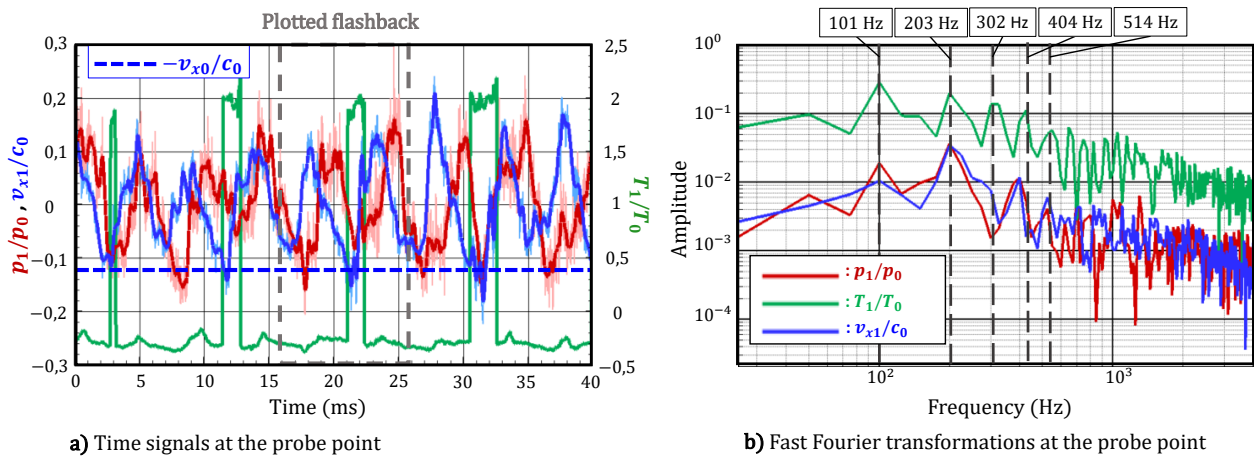


Figure 6: Pressure, temperature, and velocity signals at the probe point on the unstable case.

sponding frequency signal, computed thanks to a FFT algorithm is finally shown on fig. 6.b). As stated previously, the temperature signals main component (*i.e.* the flashback frequency) is 101 Hz (which corresponds to the combustors first natural mode[1]), whereas the pressure and velocity (bubble dilatation) essentially oscillate at 203 Hz (second natural mode), but indeed have a 101 Hz component. Significantly higher harmonics of 302, 404 and 514 Hz are also excited through non-linearities [7].

2.5 Summary

In this section, a numerical setup corresponding to a combustor featuring a backward-facing-step flame holder has been build-up, and two operating points were simulated: (*i*) a stable case, where the flame is successfully anchored

on the shear layer originating at the step, and (ii) an unstable case, where the flame does not stabilize and a massive flashback occurs periodically. Although flame motion is observed in the stable case, where the flame is wrinkled by the shear layer instability, no significant oscillations of the pressure or axial velocity are seen. The regions with high temperature oscillation being very localized in this case, the linearization of the criteria for thermoacoustic instability should work well. In the unstable case, the outlet boundary being reflective is favorable for the onset of instability as additional thermoacoustic feedback couples with the flame-hydrodynamic instability, and the pressure and axial velocity oscillations grow exponentially, which leads to periodic flashback, spreading the mean flame zone. This scenario is less propitious for linearization, as the now-spread mean flame contains vast regions with high temperature oscillation levels. As the flashback is guided by the coupling of the flame with the shear-layer, the separation bubble, and acoustic waves propagating in the whole combustors, its frequency follows the combustors first longitudinal eigenmode. Furthermore, a frequency analysis showed that a great number of higher-order harmonics are also triggered, due to the flashback mechanisms, and the second-one, which is associated with the bubble dilatation frequency, is also favoured.

3. Stability criteria

The flashback cycle being described in the previous section, several criteria for thermoacoustic instability will now be studied.

3.1 Relations between stability criteria

In section 1, it has been stated that when studying thermoacoustic instabilities, the Rayleigh criterion might not be sufficient and that the Chu criterion, or even more general non-linear criteria may be more convenient. In order to put into evidence the relation that may exist between the Rayleigh and Chu criteria, a link between temperature, pressure, and entropy oscillations should first be derived. Considering the Gibbs equation, the internal energy definition, a perfect gas and neglecting the species mass fraction variations, the following relation can be found:

$$dT = \frac{(\gamma - 1)T}{\gamma p} dp + \frac{(\gamma - 1)T}{c_p} ds \quad (7)$$

By using the previous relation, a first-order Taylor series expansion for the temperature fluctuations T_1 can easily be derived:

$$T_1 = \frac{(\gamma_0 - 1)T_0}{\gamma_0 p_0} p_1 + \frac{(\gamma_0 - 1)T_0}{\gamma_0 c_{v0}} s_1 \quad (8)$$

According to Eqs (1)–(2), the Rayleigh and Chu criteria should be equivalent if (i) the perturbation levels remains small and linearization is possible, (ii) the flow is isentropic (i.e. s_1 equals zero) and (iii) the temperature is not affected by gas composition. If linearization is possible, the Chu criterion should thus write:

$$D_{Chu} = \frac{T_1 \dot{\omega}_{T1}}{T_0} = \underbrace{\frac{\gamma_0 - 1}{\gamma_0 p_0} p_1 \dot{\omega}_{T1}}_{D_{Rayl}} + \frac{(\gamma_0 - 1)T_0}{\gamma_0 c_{v0}} s_1 \dot{\omega}_{T1} \quad (9)$$

and the Rayleigh term D_{Rayl} can be viewed as its purely acoustic part. In addition to this, in the works on non-linear disturbance energies [2, 26], the following source term for thermoacoustic coupling has been derived:

$$D_{THAC} = T_1 \left(\frac{\dot{\omega}_T}{T} \right)_1 \quad (10)$$

When decomposing the variables into their base and fluctuating components $() = ()_0 + ()_1$, this expression yields:

$$D_{THAC} = T_1 \left(\frac{\dot{\omega}_{T0} + \dot{\omega}_{T1}}{T_0 + T_1} \right)_1 = T_1 \left(\frac{\dot{\omega}_{T0}}{T_0} \left(\frac{1 + \frac{\dot{\omega}_{T1}}{\dot{\omega}_{T0}}}{1 + \frac{T_1}{T_0}} \right) \right)_1 \quad (11)$$

And by deriving the Taylor series series of the quantity $(1 + T_1/T_0)^{-1}$, one finally obtains:

$$D_{THAC}^{(n)} = \left(\frac{\dot{\omega}_{T1} T_1}{T_0} - \frac{\dot{\omega}_{T0}}{T_0^2} T_1^2 \right) - \left(\frac{\dot{\omega}_{T1} T_1^2}{T_0^2} - \frac{\dot{\omega}_{T0}}{T_0^3} T_1^3 \right) + \left(\frac{\dot{\omega}_{T1} T_1^3}{T_0^3} - \frac{\dot{\omega}_{T0}}{T_0^4} T_1^4 \right) - \left(\frac{\dot{\omega}_{T1} T_1^4}{T_0^4} - \frac{\dot{\omega}_{T0}}{T_0^5} T_1^5 \right) + \dots \quad (12)$$

Stating that the Chu term $D_{Chu} = \dot{\omega}_{T1} T_1 / T_0$ is contained in the linear second-order component of this criterion: $D_2 = (\dot{\omega}_{T1} T_1 / T_0 - \dot{\omega}_{T0} T_1^2 / T_0^2)$. The linearization of D_{THAC} also yields an additional term: $D_{T^2} = -\dot{\omega}_{T0} T_1^2 / T_0^2$, which is unconditionally damping.

It must also be recalled that these terms originally act as sources of conservation equations of the form:

$$\frac{\partial E_p}{\partial t} = D - L \quad (13)$$

stating that when neglecting the losses L , these terms act as a source for the perturbation energy E_p . The quantity D_{Rayl} is a source for the linear acoustic energy [35]. Adding entropy contribution to the linear acoustic energy, it becomes the linear fluctuating energy [6, 32], whose source is D_{Chu} , and further adding non-linear terms, it becomes the disturbance energy [26, 13], whose source is D_{THAC} . Due to the non-linear effects being mainly due to flame motion, the non-linear disturbance energy flux becomes the linear fluctuating energy flux [2], and then the linear acoustic energy flux in the far-field regions [41]. The table 3 summarizes the criteria that will be investigated in the next section.

Criterion	Expression	Definition
Non-linear	$D_{THAC} = T_1 \left(\frac{\dot{\omega}_T}{T} \right)_1$	Generalized non-linear criteria, related to the growth of non-linear disturbance energy
Total linear	$D_2 = \frac{1}{T_0} T_1 \dot{\omega}_{T1} - \frac{\dot{\omega}_{T0}}{T_0^2} T_1^2$	Linearization of D_{THAC} , contains the Chu criteria and a loss term
Chu	$D_{Chu} = \frac{1}{T_0} T_1 \dot{\omega}_{T1}$	Criteria related to the growth of the linear fluctuating energy, containing entropy disturbances
linear damping	$D_{T^2} = -\frac{\dot{\omega}_{T0}}{T_0^2} T_1^2$	Damping term appearing with the Chu criteria when linearizing D_{THAC}
Rayleigh	$D_{Rayl} = \frac{\gamma_0 - 1}{\gamma_0 p_0} p_1 \dot{\omega}_{T1}$	"Pressure contribution" in the Chu criteria, related to the growth of linear acoustic energy

Table 3: Summary of the criteria for thermoacoustic stability.

3.2 Application to the numerical simulations

The criteria mentioned above have been computed and studied in both stable and unstable cases with the same spatial and time resolution as the 2D fields of section 2 (*i.e.* 4000 extracted grids over a 40 ms interval, corresponding to 4 flashbacks for the unstable case). Figure 7 first shows the volume integrals of these various terms. The same time interval as the one described in Fig. 5 and reported in Fig. 6.a) is shown for the unstable case, with the different phases (I), (II), (III) and (I-bis) reported.

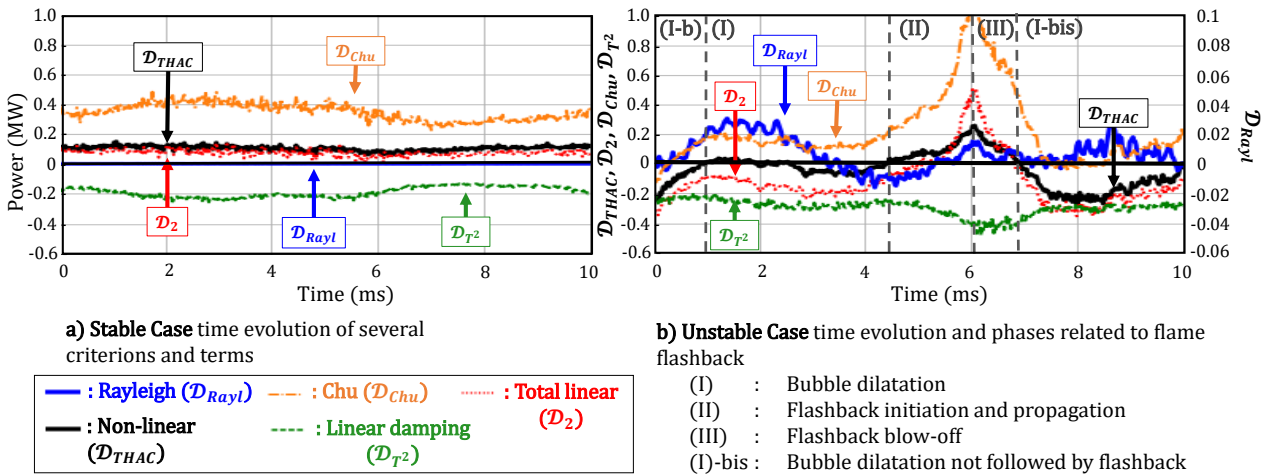


Figure 7: Global time evolution of the thermoacoustic stability criteria

In the stable case (fig. 7.a)), it can first be seen that the D_{THAC} and D_2 curves fit well, stating that global linearization works well, because the regions featuring high temperature oscillations remain very localized is the physical

space. It means that the complete non-linear term can simply be decomposed into the Chu and the linear loss terms. The first one being strictly positive, it describes the flame-induced destabilization, whereas the second one describes its damping. D_{THAC} (and D_2) being strictly positive, the flame continuously produces disturbance energy through the shear-layer instability. The Rayleigh term being negligible in this case (*i.e.*, more than 100 times smaller than D_{THAC}), flame-acoustic coupling is negligible and the destabilization is mainly due to flame-entropy coupling, *i.e.*, flame motion.

In the unstable case (fig. 7.b), D_{Chu} stays almost always positive, failing to describe the temporal re-stabilization occurring between the flashback phases. \mathcal{D}_{THAC} and \mathcal{D}_2 curves do not fit well, due to either an overestimated source or damp according to the phase, and a linear approach is thus not sufficient. On this case \mathcal{D}_{Rayl} reaches values of 40 kW, which is only about ten times smaller than \mathcal{D}_{THAC} , stating that significant acoustic energy (which equals disturbance energy in the far-field) is produced. Furthermore, the non-linear term gives precise information about the transition between several phases, whereas the Rayleigh term provides additional information about the flame acoustic couplings effects on this cycle:

- During **Phase I**, \mathcal{D}_{THAC} stays negative because the flame temporarily starts to restabilize as the recirculation zone re-establishes. A permanent restabilization is however not possible because of the bubble dilatation (and the induced unsteady heat-release) being in phase with pressure oscillations ($D_{Rayl} > 0$). The longitudinal wave (associated with the first natural mode) crossing the flame changes the pressure heat-release phasing and \mathcal{D}_{THAC} then increases whereas D_{Rayl} becomes negative, stating that acoustic energy is converted into entropy disturbance energy (*i.e.* fluctuating energy) as the flashback initiates.
- **Phase II** is characterized by \mathcal{D}_{THAC} becoming positive, meaning that disturbance energy is produced during the whole duration of the flashback. At the end of the flashback, D_{Rayl} becomes positive again and presents a peak because of the reflected acoustic wave crossing the flame again. The Rayleigh term being negative during most of this phase, the flashback propagation generates fluctuating energy rather than acoustic energy.
- \mathcal{D}_{THAC} reaches its maximum at the moment where the flame is blown-off (**Phase III**). During this phase, the fluctuating energy generated during phase II is reconverted into acoustic energy (\mathcal{D}_{THAC} decreases and becomes again negative, whereas \mathcal{D}_{Rayl} remains positive).
- The difference on **Phase I-bis** is that, due to the absence of the longitudinal wave associated with the first eigenmode, the pressure and heat-release oscillations remain in phase ($\mathcal{D}_{Rayl} > 0$), preventing the acoustic energy converting into fluctuating energy until the next dilatation, which results in \mathcal{D}_{THAC} being largely negative as the flame temporarily re-stabilizes.

The flashback cycle is maintained because the generated disturbance energy flux, which becomes essentially acoustic energy flux at the combustor boundaries, is not evacuated and keeps reflecting, giving periodically rise to the same cycle. Although the \mathcal{D}_{THAC} and \mathcal{D}_2 curves global shape is similar, when describing the flashback mechanisms, two major difficulties would be: (i): successfully predicting the initiation of the flashback, as there would roughly be a factor 2 error on the duration of phase (II), due to time lag (ii): quantifying the exact levels of the source on phases (I), (II) and (III). Using the sole Rayleigh criterion, it would also be difficult to differentiate each phase.

As it is not totally clear which is the underlying physics of the nature either as a source or a damp of \mathcal{D}_{THAC} , 2D fields of the criteria time averages are plotted in Fig. 8. The time average of one of this term being positive in a given flow region means that, on average, disturbance energy is produced and this region thus acts as a source. In order to help identifying flow regions, the same mean-temperature isolines as on figure 3 have been plotted. It can first be seen on the stable case (Fig. 8.a) that there are 2 distinct regions, stating that flame motion has a predominant role about generation of disturbance energy:

- A "burnt gas" region, below the 1900 K iso-line, where the time average of \mathcal{D}_{THAC} is strictly negative and thus acts as a damp. The reason is that a flame front convected in this region would not propagate due to the lack of reactants, thereby stabilizing the combustion. These results are consistent with the literature, as the principle of flame holding is to stabilize the flame (*i.e.* dissipating disturbance energy) through burnt gas recirculation [16].
- When the inverse occurs, a flame front will propagate in the "Fresh reactant region" (above the 1500 K isoline) which thereby acts as a source.

There is also a very thin region between these two isolines where the source time average equals zero. It can be inferred that what is playing a predominant role in this case is the motion induced through intrinsic shear layer

CRITERIA FOR THERMOACOUSTIC INSTABILITY IN COMBUSTORS FEATURING LARGE-SCALE FLAME MOTION

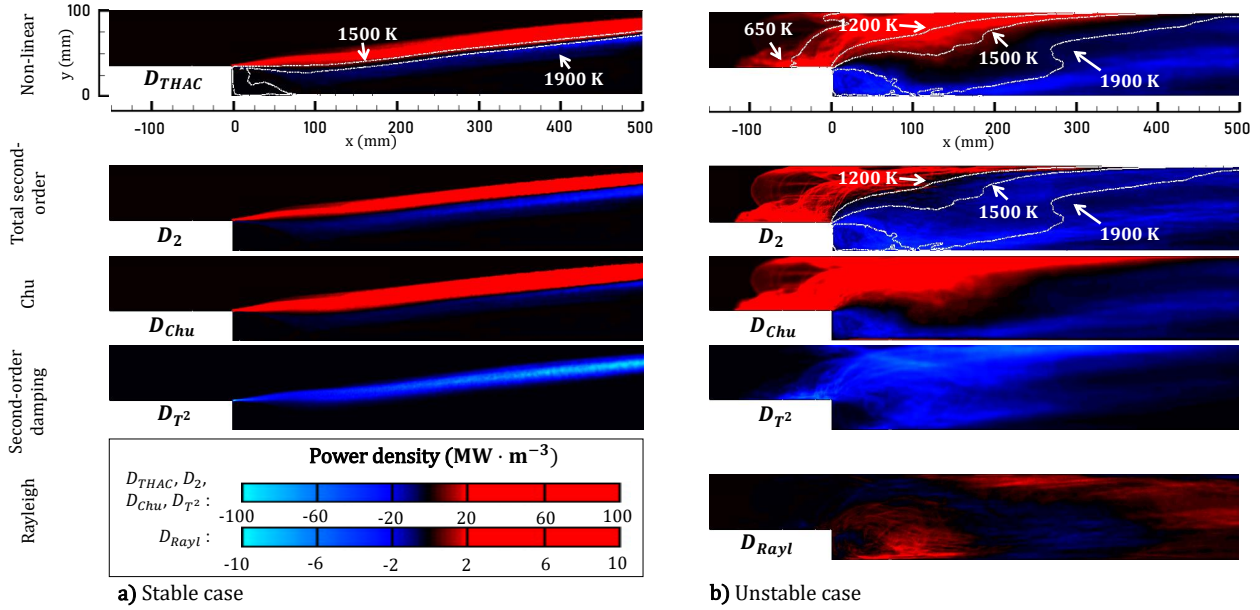


Figure 8: Local distribution of time-averaged criteria and mean temperature contours. Positive values (in red) correspond to regions where destabilization occurs

instability, *i.e.* the flame being wrinkled (the parts of the flame in burnt and fresh gases are respectively stabilizing and destabilizing). It should also be noticed that the 2D fields of D_{THAC} and D_2 are also similar in this case, and the non-linear term can thus simply be decomposed into both Chu and linear damping terms.

In the unstable case (Fig. 8.b), significant differences can be seen between D_{THAC} and D_2 , especially between the 1200 K and 1900 K isolines, stating that significant source and damping mechanisms lay in the high order terms of Eq. (11). These errors fit well with the time lag of Fig. 7, the flashback being initiated in the [1500, 1900] K region (Fig. 5-*iii*), then developing through the boundary layer in the [1200, 1500] K region (Fig. 5-*iv*), and then propagating in the core flow in the $T_0 < 1200$ K region (Fig. 5-*v*). The mechanisms driving its initiation are thus of non-linear nature, and the sole linear contributions D_{THAC} , D_{T^2} and D_2 would not be sufficient to adequately describe the flashback.

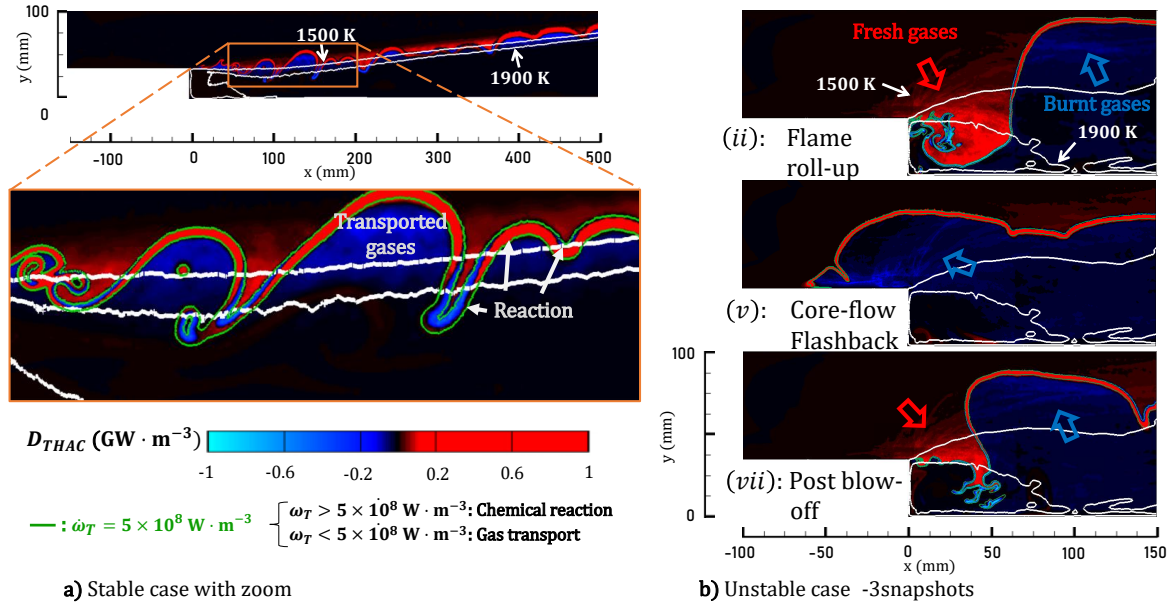
As there is a persistent damp region below the 1900 K isoline, and a persistent source above the 1500 K isoline in both cases, the instability mechanisms remain the same and are essentially related to flame motion. Whereas the instability is essentially guided by the shear-layer instability in the stable case, there is much more complex flame motion in the unstable case, where bubble dilatation, flashback, and local blow-off occurs. The Rayleigh criterion describes essentially the interaction between the bubble and acoustic waves, which is destabilizing, but does not give accurate information about the flashback.

Finally, an instantaneous snapshot of D_{THAC} is plotted for the stable case on figure 9.a). From the $\dot{\omega}_T = 5 \times 10^8 \text{ W} \cdot \text{m}^{-3}$ isoline reported in the zoom, two contributions of D_{THAC} can be distinguished:

- Chemical reaction ($\dot{\omega}_T > 5 \times 10^8 \text{ W} \cdot \text{m}^{-3}$), which as discussed previously, is relevant to the flame convection in both regions and admits respectively strictly positive and negative values in the fresh and burnt gas regions.
- Transport ($\dot{\omega}_T < 5 \times 10^8 \text{ W} \cdot \text{m}^{-3}$), which is generally in phase opposition with the above contribution. When the flame front is convected through unsteady velocity, the gas pocket behind it will be to, and the flame front will naturally propagate in fresh gas pockets (source), but not in burnt gases (damp).

The time average of D_{THAC} admitting the same sign as the first contribution in fresh and burnt gas regions (Fig. 8), the direct reaction (or flame convection) has the major role. The same mechanisms occur on the unstable case, and figure 9.b) plots D_{THAC} at three snapshots of Fig. 5. It can be seen that during flashback (*v*) and re-stabilization (*ii* & *vii*), transport of burnt gases is still stabilizing, whereas fresh gases transport is destabilizing the flow as it provokes bubble dilatation.

CRITERIA FOR THERMOACOUSTIC INSTABILITY IN COMBUSTORS FEATURING LARGE-SCALE FLAME MOTION

Figure 9: Instantaneous snapshots of D_{THAC}

3.3 Summary

The link between several criteria from the literature for thermoacoustic instability has been studied, and these criteria were then evaluated for both stable and unstable cases which have been introduced in section 2. As discussed previously, the spreading of the mean-flame through the instability is found to be decisive in the validity of the linearization, which works well only on the stable case. Further analysis on the unstable case has shown that the extended criteria (*i.e.* Chu, second-order loss, and generalized non-linear) are needed to describe the whole instability cycle. The Rayleigh criterion however gives useful information about the interaction of acoustic and disturbance energies, which plays a major role in the flashback initiation, blowing-off, and its cycle maintaining on the unstable case. The criteria have then been linked to the mechanisms involved in the combustor, and it has been established that the stabilization and destabilization through combustion-hydrodynamic coupling has the same nature in both cases and is related to flame motion in either cold reactants or burnt gases regions.

4. Conclusion

Stable and unstable combustion modes were numerically simulated for a backward-facing step flow configuration corresponding to ONERA-MICAEDI experiment. The unstable case has been numerically triggered by modifying the exit boundary reflection. Several thermoacoustic source terms for perturbation energies, describing the direct effect of heat-release dynamics have then been selected in order to construct criteria for thermoacoustic stability. The level of instability has been evaluated by using those criteria, and allowed a better understanding of the mechanisms leading to flashback. The information on the destabilization process depends on the chosen criterion:

- The Rayleigh criterion gives valuable information on the flame/acoustic waves coupling in the unstable mode but fails to describe the unsteady behaviour of the shear-layer for the stable case.
- The extended criterion proposed by Chu, which is based on a linear approach, adequately describes the flame destabilization through the unsteady shear layer on the stable case. For the unstable case, the Chu index is always positive, thus indicating the absence of stabilizing contribution to the fluctuating energy balance. This does not correspond to the observed conditions of flashback.
- On the stable case, the total linear criteria describes adequately the role of the shear-layer, with the Chu and damp term describing respectively the stabilization and destabilization mechanisms. Whereas the total linear criteria inverts its sign on the unstable case and thus takes into account some of the damping mechanisms, the non linear criteria is still needed to describe precisely the flashback time evolution.

- The non-linear approach based on Myers and Giauque's work takes into account disturbance sources of different nature (acoustic, entropic, hydrodynamic ...) and seems more relevant to describe both stable and unstable cases. It especially evidences the role of flame/hydrodynamic coupling stabilization/destabilization mechanism.

Nevertheless, the sensitivity of these results to the boundary conditions has to be evaluated. Further investigations will focus on the effect of different operating parameters such as equivalence ratio, air inlet temperature or mass flow, or wall temperature.

5. Acknowledgments

The authors gracefully acknowledge A. K. Mohamed, O. Dessornes, J. Anthoine, P. Villedieu, L. Jacquin from ONERA, and T. Coué from DGA for their support, as well as ONERA and AID (Contract DGA 2020 65 0022) for their financial support.

References

- [1] H. M. Altay, R. L. Speth, D. E. Hudgins, and A. F. Ghoniem. Flame–vortex interaction driven combustion dynamics in a backward-facing step combustor. *Combust. Flame*, 156(5):1111–1125, 2009.
- [2] M. Brear, F. Nicoud, M. Talei, A. Giauque, and E. Hawkes. Disturbance energy transport and sound production in gaseous combustion. *J. Fluid Mech.*, 707:53–73, 2012.
- [3] C. Brossard, V. Sabel'nikov, M. Orain, F. Grisch, M. Barat, A. Ristori, and P. Gicquel. Etude expérimentale des instabilités thermo-acoustiques d'une flamme turbulente prémélangée.
- [4] J. C. Butcher. Implicit Runge-Kutta processes. *Math. Comp.*, 18(85):50–64, 1964.
- [5] L. Chen, K. Asai, T. Nonomura, G. Xi, and T. Liu. A review of backward-facing step (BFS) flow mechanisms, heat transfer and control. *Therm. Sci. and Eng. Prog.*, 6:194–216, 2018.
- [6] B.T. Chu. On the energy transfer to small disturbances in fluid flow (part I). *Acta Mechanica*, 1(3):215–234, 1965.
- [7] F.E.C. Culick and V. Yang. Prediction of the stability of unsteady motions in solid-propellant rocket motors. 1992.
- [8] P. G. Drazin and W. H. Reid. *Hydrodynamic stability*. Cambridge university press, 2004.
- [9] A. Er-Raiy, Z. Bouali, J. Reveillon, and A. Mura. Optimized single-step (OSS) chemistry models for the simulation of turbulent premixed flame propagation. *Combust. Flame*, 192:130–148, 2018.
- [10] R. S. Fry. A century of ramjet propulsion technology evolution. *J. Propul. Power*, 20(1):27–58, 2004.
- [11] K. J. George and R.I. Sujith. On chu's disturbance energy. *J. Sound Vib.*, 330(22):5280–5291, 2011.
- [12] A. Giauque. *Fonctions de transfert de flamme et énergies des perturbations dans les écoulements réactifs*. PhD thesis, Toulouse, INPT, 2007.
- [13] A. Giauque, T. Poinso, M. Brear, and F. Nicoud. Budget of disturbance energy in gaseous reacting flows. In *Proc. Summer Program*, pages 285–297. Center for Turbulence Research, NASA Ames/Stanford Univ., 2006.
- [14] D.G. Goodwin. Cantera C++ users guide. *California Institute of Technology*, 2002.
- [15] A. Kalantari and V. McDonell. Boundary layer flashback of non-swirling premixed flames: Mechanisms, fundamental research, and recent advances. *Prog. Energy Combust. Sci.*, 61:249–292, 2017.
- [16] K. S. Kedia and A. F. Ghoniem. The anchoring mechanism of a bluff-body stabilized laminar premixed flame. *Combust. Flame*, 161(9):2327–2339, 2014.
- [17] J.O. Keller, L. Vaneveld, D. Korschelt, G.L. Hubbard, A.F. Ghoniem, J.W. Daily, and A.K. Oppenheim. Mechanism of instabilities in turbulent combustion leading to flashback. *AIAA J.*, 20(2):254–262, 1982.

- [18] H. Y. Ken, A. Trouvé, and J. W. Daily. Low-frequency pressure oscillations in a model ramjet combustor. *J. Fluid Mech.*, 232:47–72, 1991.
- [19] C. Le Touze, A. Murrone, and H. Guillard. Multislope MUSCL method for general unstructured meshes. *J. Comp. Phys.*, 284:389–418, 2015.
- [20] J-P. Legier, T. Poinso, and D. Veynante. Dynamically thickened flame les model for premixed and non-premixed turbulent combustion. In *Proc. Summer Program*, volume 12. Center for Turbulence Research Stanford, CA, 2000.
- [21] T. C. Lieuwen. *Unsteady combustor physics*. Cambridge University Press, 2012.
- [22] G. Linassier, A. Bruyat, P. Villedieu, N. Bertier, C. Laurent, O. Rouzaud, R. Lecourt, H. Verdier, and G. Lavergne. Application of numerical simulations to predict aircraft combustor ignition. *CR Mecanique*, 341(1-2):201–210, 2013.
- [23] Y. Méry. Dynamical response of a perfectly premixed flame and limit behavior for high power density systems. *Combust. Flame*, 192:410–425, 2018.
- [24] C.L. Morfey. Acoustic energy in non-uniform flows. *J. Sound Vib.*, 14(2):159–170, 1971.
- [25] Y. Moule, V.r. Sabel'nikov, A. Mura, and M. Smart. Computational fluid dynamics investigation of a mach 12 scramjet engine. *J. Propul Power*, 30(2):461–473, 2014.
- [26] M.K. Myers. Transport of energy by disturbances in arbitrary steady flows. *J. Fluid Mech.*, 226:383–400, 1991.
- [27] F. Nicoud and F. Ducros. Subgrid-scale stress modelling based on the square of the velocity gradient tensor. *Flow Turb. Combust.*, 62(3):183–200, 1999.
- [28] F. Nicoud and T. Poinso. Thermoacoustic instabilities: Should the Rayleigh criterion be extended to include entropy changes? *Combust. Flame*, 142(1-2):153–159, 2005.
- [29] N. Petrova. *Turbulence-chemistry interaction models for numerical simulation of aeronautical propulsion systems*. PhD thesis, Ecole polytechnique X, 2015.
- [30] U. Piomelli. Large-eddy simulation: achievements and challenges. *Prog. Aerospace Sci.*, 35(4):335–362, 1999.
- [31] U. Piomelli and E. Balaras. Wall-layer models for large-eddy simulations. *Annu. Rev. Fluid Mech.*, 34(1):349–374, 2002.
- [32] T. Poinso and D. Veynante. *Theoretical and numerical combustion*. RT Edwards, Inc., 2005.
- [33] S. B. Pope. *Turbulent flows*. Cambridge university press, 2000.
- [34] J.W.S. Rayleigh. The explanation of certain acoustical phenomena. *Roy. Inst. Proc.*, 8:536–542, 1878.
- [35] J.W.S. Rayleigh. The theory of sound. 1896. *Vib. plates*, 1:270–272, 1945.
- [36] A. Refloch, B. Courbet, A. Murrone, P. Villedieu, C. Laurent, P. Gilbank, J. Troyes, L. Tessé, G. Chaineray, J-B. Dargaud, et al. Cedre software. *AerospaceLab*, (2):p–1, 2011.
- [37] S. W. Rienstra and A. Hirschberg. An introduction to acoustics. *Eindhoven University of Technology*, 18:19, 2004.
- [38] B. Sainte-Rose. *Simulations numériques d'écoulements réactifs massivement décollés par une approche hybride RANS/LES*. PhD thesis, Châtenay-Malabry, Ecole Centrale de Paris, 2010.
- [39] W.C. Strahle. On combustion generated noise. In *7th Propulsion Joint Specialist Conference*, page 735, 1971.
- [40] R.I. Sujith, M.P. Juniper, and P.J. Schmid. Non-normality and nonlinearity in thermoacoustic instabilities. *Int. J. Spray Combust. Dyn.*, 8(2):119–146, 2016.
- [41] M. Talei, M. Brear, F. Nicoud, D. Bodony, and A. Giauque. Transport of disturbance energy in hot and cold turbulent jets. In *13th AIAA/CEAS Aeroacoustics Conference (28th AIAA Aeroacoustics Conference)*, page 3633, 2007.

CRITERIA FOR THERMOACOUSTIC INSTABILITY IN COMBUSTORS FEATURING LARGE-SCALE FLAME MOTION

- [42] P. S. Volpiani, T. Schmitt, and D. Veynante. Large eddy simulation of a turbulent swirling premixed flame coupling the tfiles model with a dynamic wrinkling formulation. *Combust. Flame*, 180:124–135, 2017.
- [43] F. A. Williams. *Combustion theory*. CRC Press, 2018.
- [44] C. S. Yoo, Y. Wang, A. Trouvé, and H. G. Im. Characteristic boundary conditions for direct simulations of turbulent counterflow flames. *Combust. Theor. Model.*, 9(4):617–646, 2005.